Vítor Monteiro, J. G. Pinto, Tiago J. C. Sousa, Andrés A. Nogueiras Meléndez, João L. Afonso

"A Novel Single-Phase Five-Level Active Rectifier for On-Board EV Battery Chargers"

IEEE ISIE International Symposium on Industrial Electronics, Scotland UK, pp.582-587, June 2017.

http://ieeexplore.ieee.org/document/8001311/

ISBN: 978-1-5090-1411-8

DOI: 10.1007/978-3-319-60285-1_25

Vítor Monteiro, J. G. Pinto, Tiago J. C. Sousa, Andrés A. Nogueiras Meléndez, João L. Afonso, "A Novel Single-Phase Five-Level Active Rectifier for On-Board EV Battery Chargers", IEEE ISIE International Symposium on Industrial Electronics, Scotland UK, pp.582-587, June 2017. DOI 10.1109/ISIE.2017.8001311 ISBN 978-150901412-5 ISSN 2163-5145

A Novel Single-Phase Five-Level Active Rectifier for On-Board EV Battery Chargers

Vítor Monteiro[1], J. G. Pinto[1], Andrés A. Nogueiras Meléndez[2], João L. Afonso[1]
[1]ALGORITMI Research Centre – University of Minho, Guimarães – Portugal
[2]Departamento de Tecnología Electrónica – University of Vigo, Vigo – Spain
[1]{vitor.monteiro | gabriel.pinto | joao.l.afonso}@algoritmi.uminho.pt [2]aaugusto@uvigo.es

***Abstract*—This paper presents a novel single-phase active rectifier for applications of on-board EV battery chargers. The proposed active rectifier, with reduced number of semiconductors, is constituted by four MOSFETs and four diodes, and can produce five distinct voltage levels, allowing to reduce the passive filters used to interface with the electrical power grid. An almost sinusoidal grid current with unitary power factor is achieved in the grid side for all the operating power range, contributing to preserve the power quality. The principle of operation, the current control strategy and the modulation technique are presented in detail. Simulation results in different conditions of operation are presented to highlight the feasibility and advantages of the proposed active rectifier.**

Keywords—EV Battery Charger; Five-Level Active Rectifier; Power Quality; Sinusoidal Grid Current.

I. INTRODUCTION

Active rectifiers gained notoriety in several applications, mainly, due to the contribution to preserve some power quality aspects as the low total harmonic distortion of the grid current and the unitary power factor [1]. Therefore, active rectifiers are also identified as power-factor-correction (PFC) converters. PFC converters for on-board EV battery chargers are proposed in [2], [3], [4], [5] and [6], a PFC for motor drive applications is proposed in [7], a PFC for minimizing life cycle cost in data centers is proposed in [8], and a PFC in electronic ballasts for lighting applications is proposed in [9].

The more usual active rectifier identified in the literature is composed by a full-bridge diode rectifier followed by a dc-dc boost converter with controlled input current. Reviews about PFC active rectifiers using the boost converter are presented in [10], [11] and [12]. Besides the boost converter, other dc-dc converters for the same purpose can be used. A PFC with the buck converter is proposed in [13], a PFC with a dc-dc flyback is proposed in [14], a PFC with a full-bridge is proposed in [15] and in [16], a PFC with the Ćuk converter is presented in [17], a PFC using three-state cells is proposed in [18], and a review of PFC converters based on the buck, buck-boost and forward is presented in [19]. Besides, a new family of isolated PFC active rectifiers is proposed in [20]. In order to avoid the use of the diode full-bridge front-end converter and to optimize the efficiency comparing with the traditional PFC (boost converter), a set of PFC bridgeless converters is proposed in [21], a buck-type PFC bridgeless is proposed in [22], and a buck-boost PFC bridgeless is proposed in [23].

Depending on the type of application, multilevel active rectifiers are used to decrease the size of passive components and consequently to decrease the cost of the application. Moreover, multilevel active rectifiers are also an optimal solution for applications with several dc-link interfaces. Taking into account that voltage-source active rectifiers connected to the power grid produce a voltage in order to control the grid current, improving the produced voltage allows to improve the grid current. The produced voltage can be improved increasing the number of voltage levels allowed by the PFC active rectifier. However, the increase in the number of voltage levels requires more hardware components, namely, power semiconductors, gate-drivers and voltage sensors, and cannot be feasible for on-board EV battery chargers. Exhaustive reviews about multilevel converters, power control theories and applications are presented in [24] and [25]. By combining PFC multilevel active rectifiers in series, it is possible to increase significantly the number of voltage levels. However, the main disadvantage is the number of independent dc-link outputs. This family of converters is identified in the literature as modular multilevel converters. Complete reviews about the principle of operation, the control strategy and the applications of the modular multilevel converters are presented in [26] and [27].

In this context, this paper proposes a novel multilevel active rectifier capable to produce five distinct voltage levels to operate as front-end converter for on-board EV battery chargers. The proposed active rectifier is presented in Fig. 1. Comparing with the main five-level active rectifiers identified in the literature [28][29][30][31][32], the main advantages of the proposed active rectifier are: reduced number of semiconductors to produce five distinct voltage levels; single output dc-link with split capacitors, which is fundamental for on-board EV battery chargers; and semi-bridgeless topology without flying capacitors and cascade converters. The detailed principle of operation is presented in section II and the digital control design, including the grid current control strategy and the modulation technique is presented in section III. A detailed

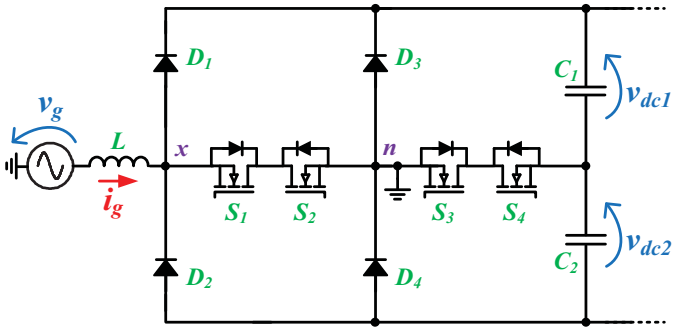

Fig. 1. Proposed five-level active rectifier for on-board EV battery chargers.

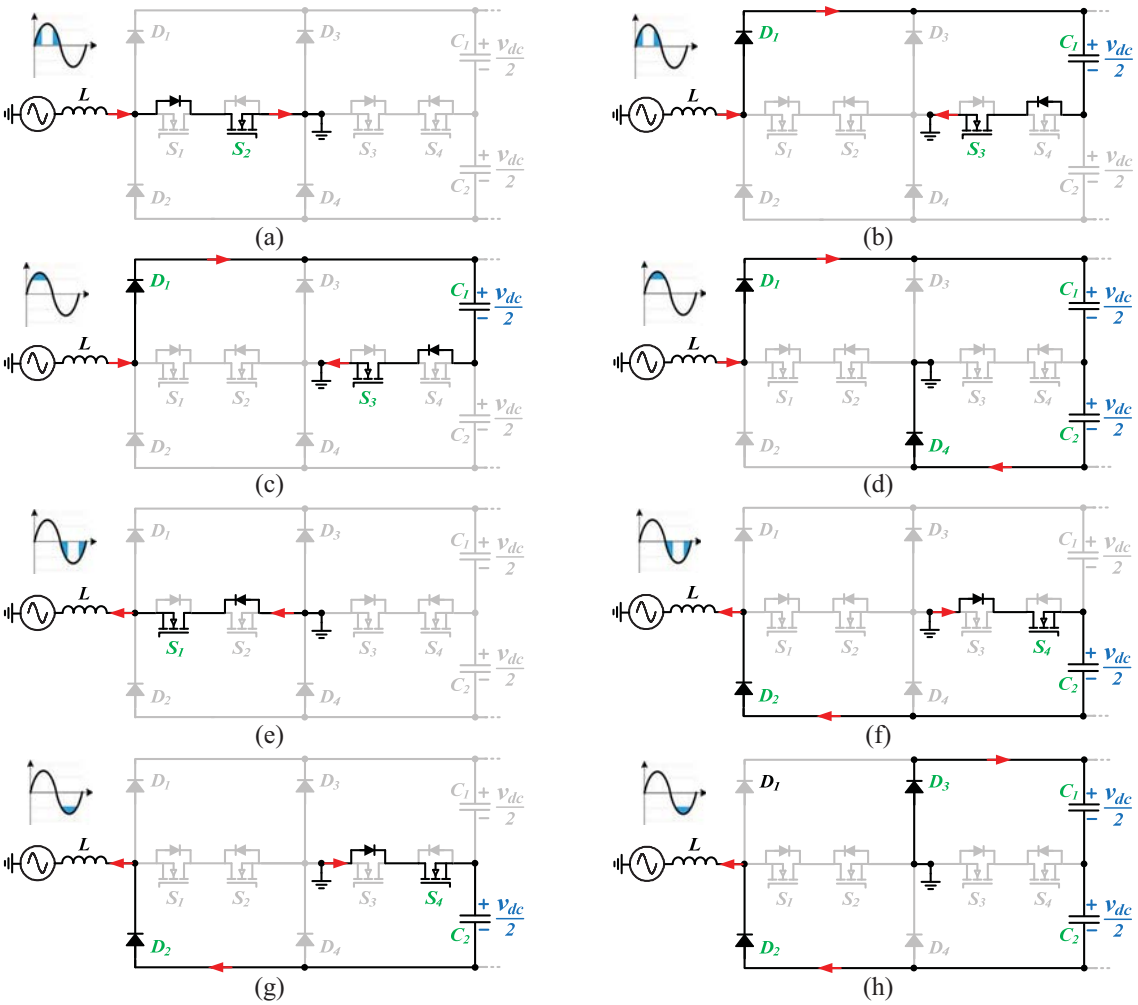

Fig. 2. Stages of operation of the proposed single-phase five-level active rectifier: (a) v_{ar} = 0 V - when the produced voltage varies between 0 and $+v_{dc}/2$; (b) $v_{ar} = +v_{dc}/2$ V - when the produced voltage varies between 0 and $+v_{dc}/2$; (c) $v_{ar} = +v_{dc}/2$ V - when the produced voltage varies between $+v_{dc}/2$ and $+v_{dc}$; (d) $v_{ar} = +v_{dc}$ V - when the produced voltage varies between $+v_{dc}/2$ and $+v_{dc}$; (e) v_{ar} = 0 V - when the produced voltage varies between 0 and $-v_{dc}/2$; (f) $v_{ar} = -v_{dc}/2$ V - when the produced voltage varies between 0 and $-v_{dc}/2$; (g) $v_{ar} = -v_{dc}/2$ V - when the produced voltage varies between $-v_{dc}/2$ and $-v_{dc}$; (h) $v_{ar} = -v_{dc}$ V - when the produced voltage varies between $-v_{dc}/2$ and $-v_{dc}$.

and comprehensive validation of the proposed active rectifier is presented in section IV and the main conclusions are presented in section V.

II. Principle of Operation

The principle of operation is presented in this section. The proposed active rectifier allows to produce five distinct voltage levels ($+v_{dc}$, $+v_{dc}/2$, 0, $-v_{dc}/2$ and $-v_{dc}$), i.e., the voltage between the points x and n identified in Fig. 1. The analysis is performed for two quadrants, i.e., positive voltage with positive current, and negative voltage with negative current.

During the positive half-cycle the MOSFETs S_1 and S_4 are always OFF. When the voltage produced by the active rectifier varies between 0 and $+v_{dc}/2$ are switched the MOSFETs S_2 and S_3. When the MOSFET S_2 is ON and the MOSFET S_3 is OFF the voltage produced is 0 (cf. Fig. 2(a)), and when the MOSFET S_2 is OFF and the MOSFET S_3 is ON the voltage produced is $+v_{dc}/2$ (cf. Fig. 2(b)). When the voltage produced by the active rectifier varies between $+v_{dc}/2$ and $+v_{dc}$, the MOSFET S_2 is OFF and the MOSFET S_3 is switched. When the MOSFET S_3 is ON the voltage produced is $+v_{dc}/2$ (cf. Fig. 2(c)), and when the MOSFET S_3 is OFF the voltage produced is $+v_{dc}$ (cf. Fig. 2(d)). On the other hand, during the negative half-cycle the MOSFETs S_2 and S_3 are always OFF. When the voltage produced by the active rectifier varies between 0 and $-v_{dc}/2$ are switched the MOSFETs S_1 and S_4. When the MOSFET S_1 is ON and the MOSFET S_4 is OFF the voltage produced is 0 (cf. Fig. 2(e)), and when the MOSFET S_1 is OFF and the MOSFET S_4 is ON the voltage produced is $-v_{dc}/2$ (cf. Fig. 2(f)). When the voltage produced by the active rectifier varies between $-v_{dc}/2$ and $-v_{dc}$, the MOSFET S_1 is OFF and the MOSFET S_4 is switched. When the MOSFET S_4 is ON the voltage produced is $-v_{dc}/2$ (cf. Fig. 2(g)), and when the MOSFET S_4 is OFF the voltage produced is $-v_{dc}$ (cf. Fig. 2(h)).

The operation stages of the proposed active rectifier during the positive and negative half-cycles to produce the five distinct voltage levels are presented in Fig. 2, and the switching states are summarized in Table I. It is important to note that, when the MOSFETs are OFF, the maximum voltage applied to each one is $v_{dc}/2$. Fig. 3 shows the power grid voltage (v_g), the grid current (i_g), the voltage produced by the active rectifier (v_{ar}), the MOSFETs pulse-pattern (S_1, S_2, S_3 and S_4), the

TABLE I
SWITCHING STATES OF THE PROPOSED FIVE-LEVEL ACTIVE RECTIFIER

Voltage v_g	MOSFET S_1	S_2	S_3	S_4	Level v_{ar}
$v_g > 0$	OFF	ON	OFF	OFF	0
	OFF	OFF	ON	OFF	$+v_{dc}/2$
	OFF	OFF	ON	OFF	$+v_{dc}/2$
	OFF	OFF	OFF	OFF	$+v_{dc}$
$v_g < 0$	ON	OFF	OFF	OFF	0
	OFF	OFF	OFF	ON	$-v_{dc}/2$
	OFF	OFF	OFF	ON	$-v_{dc}/2$
	OFF	OFF	OFF	OFF	$-v_{dc}$

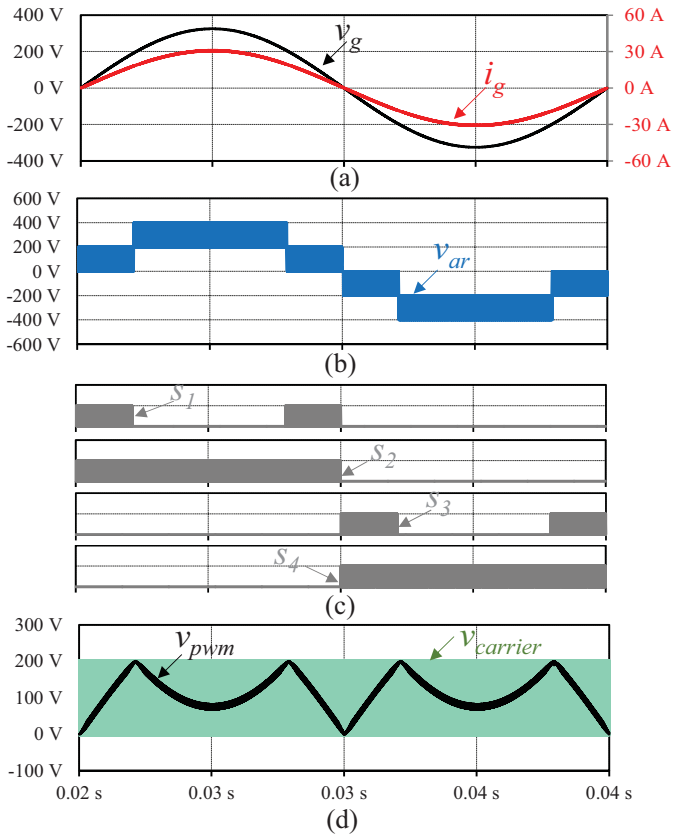

Fig. 3. Simulation results of the proposed active rectifier: (a) Power grid voltage (v_g) and grid current (i_g); (b) Voltage produced by the active rectifier (v_{ar}); (c) MOSFETs pulse-patterns (S_1, S_2, S_3 and S_4); (d) Triangular carrier ($v_{carrier}$) and signal that is compared with the carrier (v_{pwm}).

triangular carrier ($v_{carrier}$) and the signal that is compared with the carrier (v_{pwm}). As shown, the active rectifier operates with unitary power factor, i.e., the power grid voltage (v_g) and the grid current (i_g) are in phase, and the five voltage levels (v_{ar}) are clearly identified. It is important to note that is used a modified sinusoidal PWM in order to establish the pulse-pattern for each MOSFET.

III. DIGITAL CONTROLLER DESIGN

This section presents the control algorithm of the proposed active rectifier, i.e., the dc-link voltage control and the strategy to control the grid current. Taking into account that the grid current is directly influenced by the operating power, the grid current reference (i_g*) is established according to:

TABLE II
MAIN PARAMETERS OF THE SIMULATION MODEL

Parameter	Value	Unit
Power Grid Voltage	230	V
Power Grid Frequency	50	Hz
Maximum Power	5	kW
Maximum Dc-Link Voltage	400	V
Switching Frequency	100	kHz
Sampling Frequency	200	kHz
Input Inductor	300	µH
Dc-Link Capacitor	3	mF

$$i_g^*[k] = \frac{p_{dc}[k] + p_{load}[k]}{V_G^2} v_{g1}[k], \quad (1)$$

where, V_G is the rms value and v_{g1} the instantaneous value of the power grid voltage fundamental component, p_{load} the power of the load (dc-dc back-end converter of the EV battery charger) and p_{dc} the power necessary to maintain the dc-link voltage regulated. Taking into account the structure of the dc-link, the voltage of the capacitor C_1 is adjusted during the positive half-cycle of the power grid voltage and the voltage of the capacitor C_2 is adjusted during the negative half-cycle. In order to control such voltages (v_{dc1} and v_{dc2}), digital PI controllers are used, according to:

$$v_{dc1,2\_error}[k] = v_{dc1,2}^*[k] - v_{dc1,2}[k], \quad (2)$$

$$v_{dc1,2\_int}[k] = v_{dc1,2_{int}}[k-1] + v_{dc1,2\_error}[k], \quad (3)$$

$$v_{dc1,2\_PI}[k] = k_p v_{dc1,2\_error}[k] - k_i v_{dc1,2\_int}[k], \quad (4)$$

where, $v_{dc1,2\_error}$ is the error between the voltage reference (v_{dc}*) and the measured voltage ($v_{dc1,2}$), $v_{dc1,2\_int}$ denotes the integral of the $v_{dc1,2\_error}$, $v_{dc1,2\_PI}$ the output of the PI controller, and k_p and k_i gains. In order to obtain a sinusoidal grid current reference, instead of use directly the measured dc-link voltages (v_{dc1} and v_{dc2}) is used a low-pass digital filter. Taking into account that the proposed active rectifier produces a voltage (v_{ar}) to control the grid current (i_g) according to the reference (i_g*), the equation that relates these variables is established according to:

$$v_{ar}[k] = v_g[k] - L f_s\left(i_g^*[k] - i_g[k]\right), \quad (5)$$

where, L is the value of the coupling inductor between the active rectifier and the power grid and f_s is the sampling frequency of the digital controller. It is important to note that the active rectifier is synchronized with the power grid voltage through a phase-locked loop [33]. With the variables v_{ar}, v_{dc1}*, v_{dc2}*, and v_g are selected the states of the MOSFETs according to the switching technique described in section II.

IV. ANALYSIS AND SIMULATIONS

The proposed active rectifier was validated through computer simulations using the PSIM v9.0 software. The main parameters of the simulation model are presented in Table II. Fig. 4 shows the simulation results of the proposed active rectifier. Fig. 4(a) shows the power grid voltage (v_g), the grid current (i_g), and the voltage produced by the active rectifier

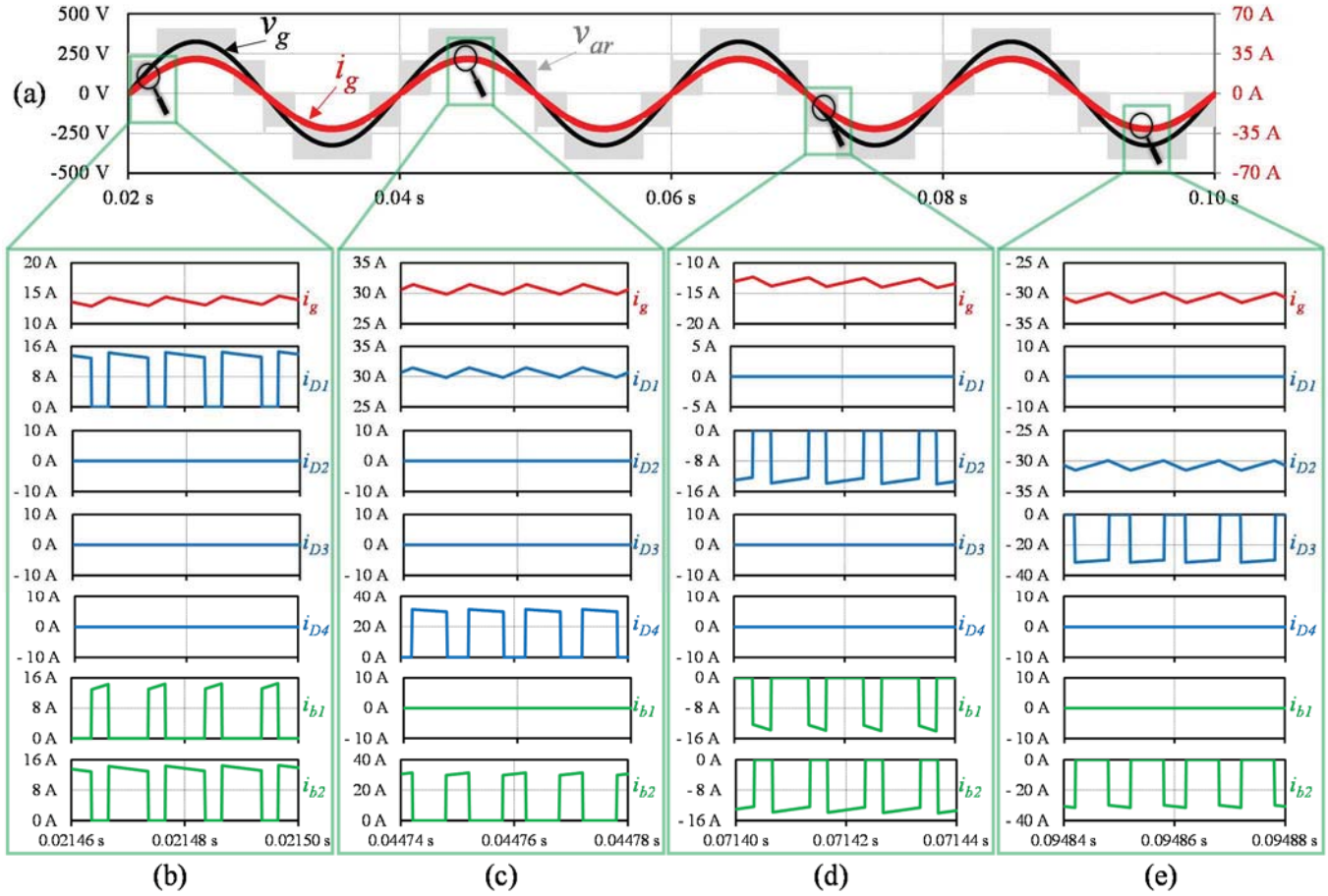

Fig. 4. Simulation results of the proposed active rectifier: (a) Power grid voltage (v_g), grid current (i_g) and voltage produced by the active rectifier (v_{ar}); (b) (c) (d) (e): Circulating currents in the active rectifier (i_g, i_{D1}, i_{D2}, i_{D3}, i_{D4}, i_{b1} and i_{b2}) according to the different voltage levels.

(v_{ar}). Fig. 4(b), Fig. 4(c), Fig. 4(d), and Fig. 4(e) shows in detail all the circulating currents in the active rectifier according to the different voltage levels produced. During the positive half-cycle, when the voltage v_{ar} varies between 0 and $+v_{dc}/2$, the current in the diodes D_2, D_3 and D_4 is 0, the current in the diode D_1 (i_{D1}) is equal to the current in the bidirectional switch, formed by the MOSFETs S_3 and S_4, (i_{b2}) and the grid current (i_g) is the sum of i_{b2} with the current in the MOSFETs S_1 and S_2 (i_{b1}). These currents are shown in detail in Fig. 4(b). Also during the positive half-cycle, when the voltage v_{ar} varies between $+v_{dc}/2$ and $+v_{dc}$, the current in the diodes D_2 and D_3 is 0, the current in the diode D_1 (i_{D1}) is equal to the grid current (i_g), which is composed by the sum of the current in the diode D_4 (i_{D4}) with the current in the MOSFETs S_3 and S_4 (i_{b2}). During this interval, the current in the MOSFETs S_1 and S_2 (i_{b1}) is also 0. These currents are shown in detail in Fig. 4(c). During the negative half-cycle, when the voltage v_{ar} varies between 0 and $-v_{dc}/2$, the current in the diodes D_1, D_3 and D_4 is 0, the current in the diode D_2 (i_{D2}) is equal to the current in the MOSFETs S_3 and S_4 (i_{b2}) and the grid current (i_g) is the sum of i_{b2} with the current in the MOSFETs S_1 and S_2 (i_{b1}). These currents are shown in detail in Fig. 4(d). Also during the negative half-cycle, when the voltage v_{ar} varies between $-v_{dc}/2$ and $-v_{dc}$, the current in the diodes D_1 and D_4 is 0, the current in the diode D_2 (i_{D2}) is equal to the grid current (i_g), which is composed by the sum of the current in the diode D_3 (i_{D3}) with the current in the MOSFETs S_3 and S_4 (i_{b2}). During this interval, the current in the MOSFETs S_1 and S_2 (i_{b1}) is also 0. These currents are shown in detail in Fig. 4(e).

Fig. 5 shows, during a time interval of 300 ms, the dc-link voltages (v_{dc1} and v_{dc2}), the power grid voltage (v_g), and the grid current (i_g). In order to approximate the simulation model to realistic operating conditions, a power grid voltage with a total harmonic distortion of 2% was used, as well as a dc-dc back-end converter to simulate different operating powers. These simulation results were obtained in order to validate the proposed active rectifier operating as an ac-dc front-end converter in an on-board EV battery charger, i.e., operating with variable power. The simulation starts with a reference power of 1 kW, at t = 0.12 s the reference power changes to 3 kW, and at t = 0.265 the power reference changes to the nominal power of 5 kW. As shown, during the three stages the dc-link voltages in both capacitors (v_{dc1} and v_{dc2}) oscillates around the reference voltage (200 V) and the ripple depends on the power of the converter, i.e., if the power increases (due to the dc-dc back-end converter), then the ripple in the dc-link voltages also increases. Due to the PLL algorithm and the low-pass digital filter (in the dc-link voltages) used in the control algorithm (cf. section III), the grid current (i_g) is almost sinusoidal and in phase with the power grid voltage (v_g), during the three operating power stages. A detailed visualization of the

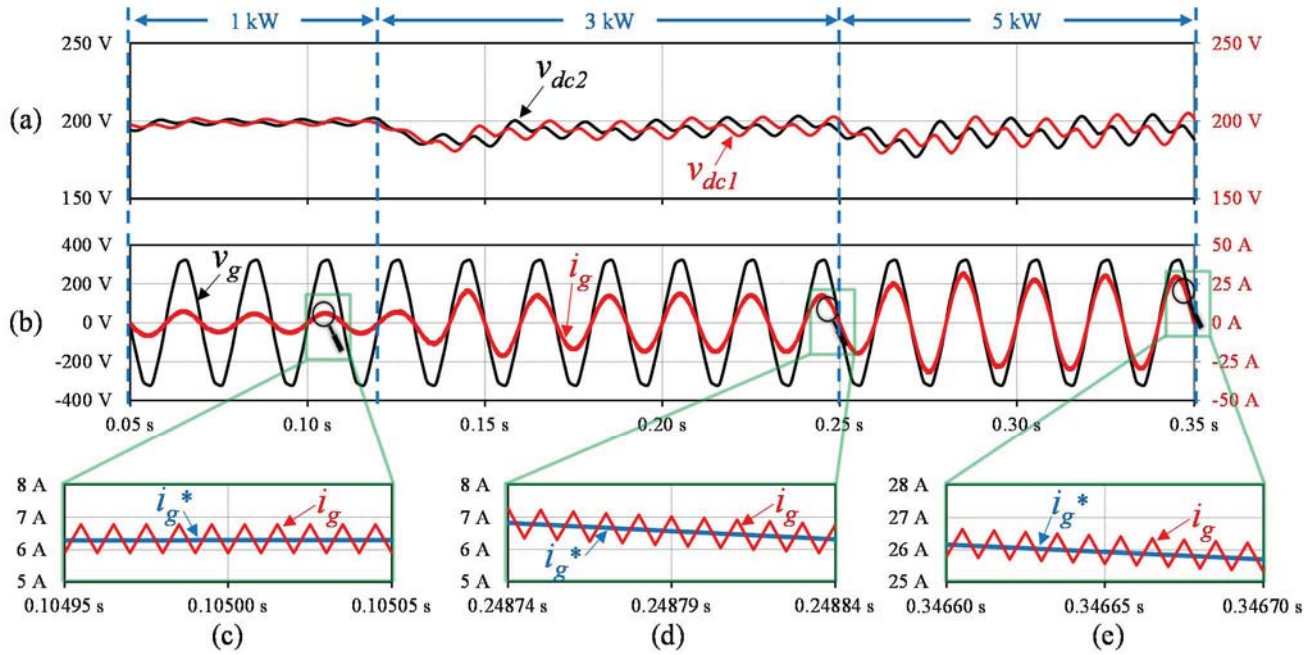

Fig. 5. Simulation results of the proposed active rectifier: (a) Dc-link voltages (v_{dc1} and v_{dc2}); (b) Power grid voltage (v_g) with a THD% of 2% and grid current (i_g); (c) (d) (e) Details of the grid current (i_g) and its reference (i_g*) for three operating powers (respectively, 1 kW, 2 kW, and 5 kW).

grid current (i_g), as well as a comparison between the grid current (i_g) and its reference (i_g*) for three operating powers, is shown in Fig. 5(c), Fig. 5(d) and Fig. 5(e). A comparison between the proposed active rectifier and the traditional PFC converter applied in EV battery chargers (full-bridge diodes followed by a dc-dc boost converter) was established. Both converters were simulated connected to the power grid voltage with an rms value of 230 V and under the same operating conditions, i.e., nominal power of 5 kW, and the same passive filters, switching frequency, sampling frequency, and grid current control strategy. Fig. 6 shows, during a time interval of 50 ms, the power grid voltage (v_g) and the obtained grid current for both converters under comparison. A detailed visualization between the obtained grid current using both converters under comparison and the determined reference is shown in Fig. 6(b). From this result is possible to verify that the grid current ripple is more reduced using the proposed active rectifier, representing an important advantage in terms of sizing and optimization of the passive filters used as interface with the power grid. Fig. 7 shows the THD% of the grid current using both converters under comparison for a range of operating power between 1 kW and 5 kW and for a THD% of the power grid voltage of 2%. As expected, in both cases, the THD% decreases as the operating power increases and is not influenced by the THD% of the power grid voltage due to the control strategy (cf. section III). As shown, the THD% is lower using the proposed active rectifier for all the operating powers. The reduced THD% of the proposed active rectifier represents an important advantage for EV battery chargers connected into the power grid.

V. Conclusion

A novel single-phase five-level active rectifier for on-board EV battery chargers is presented. The proposed topology presents advantages when compared with more conventional

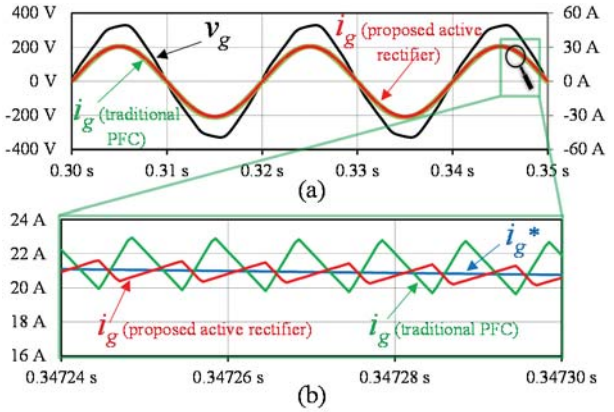

Fig. 6. Simulation results: (a) Power grid voltage (v_g), grid current of the proposed active rectifier and grid current of the traditional PFC; (b) Detailed comparison of the grid current with its reference (i_g*).

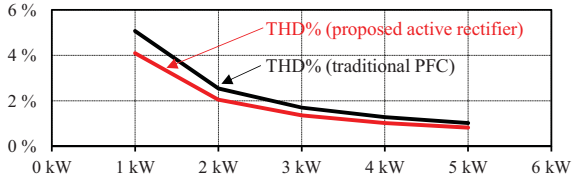

Fig. 7. Simulation results of the grid current THD% for an operating power range between 1 kW and 5 kW, and for a power grid voltage THD% of 2%.

active rectifiers used for the same applications. Since it produces five distinct voltage levels, it allows to reduce the values of the passive filters used to interface with the power grid. The proposed active rectifier was validated through computer simulations considering realistic operating conditions, e.g., a power grid voltage with a THD% of 2% and a dc-dc back-end converter with operating powers from 1 kW to 5 kW. A comparison with a traditional solution for on-board EV battery chargers was established. The maximum measured THD% of the grid current was 4.1% for an operating power of

1 kW, and the minimum THD% was 0.82% for the nominal power of 5 kW. For all the operating powers, an almost sinusoidal grid current with unitary power factor is achieved, contributing to preserve the power quality associated with the integration of EVs into the electrical power grid.

ACKNOWLEDGMENT

This work has been supported by COMPETE: POCI-01-0145-FEDER-007043 and FCT within the Project Scope: UID/CEC/00319/2013. This work is financed by the ERDF – European Regional Development Fund through the Operational Programme for Competitiveness and Internationalisation - COMPETE 2020 Programme, and by National Funds through the Portuguese funding agency, FCT - Fundação para a Ciência e a Tecnologia, within project SAICTPAC/0004/2015-POCI-01-0145-FEDER-016434.

REFERENCES

[1] Bhim Singh, Brij N. Singh, Ambrish Chandra, Kamal Al-Haddad, Ashish Pandey, Dwarka P. Kothari, "A Review of Single-Phase Improved Power Quality AC-DC Converters," IEEE Trans. Ind. Electron., vol.50, no.5, pp.962-981, Oct. 2003.

[2] Deepak S. Gautam, Fariborz Musavi, Murray Edington, Wilson Eberle, William G. Dunford, "An Automotive Onboard 3.3-kW Battery Charger for PHEV Application," IEEE Trans. Veh. Technol., vol.61, no.8, pp.3466-3474, Oct. 2012.

[3] T. B. Soeiro, T. Friedli, J. W. Kolar, "SWISS Rectifier – A Novel Three-Phase Buck-Type PFC Topology for Electric Vehicle Battery Charging," IEEE Applied Power Electronics Conference and Exposition, pp. 2617-2624, Feb. 2012.

[4] Vítor Monteiro, Bruno Exposto, João C. Ferreira, João Luiz Afonso, "Improved Vehicle-to-Home (iV2H) Operation Mode: Experimental Analysis of the Electric Vehicle as Off-Line UPS," IEEE Trans. Smart Grid, 2016.

[5] Vítor Monteiro, Andrés A. Nogueiras Meléndez, Carlos Couto, João L. Afonso, "Model Predictive Current Control of a Proposed Single-Switch Three-Level Active Rectifier Applied to EV Battery Chargers," IEEE IECON Industrial Electronics Conference, pp.1365-1370, Oct. 2016.

[6] Hani Vahedi, Philippe-Alexandre Labbé, Kamal Al-Haddad, "Single-Phase Single-Switch Vienna Rectifier as Electric Vehicle PFC Battery Charger," IEEE VPPC Vehicle Power and Propulsion Conference, pp.1-6, Oct. 2015.

[7] Vashist Bist, Bhim Singh, "PFC Cuk Converter-Fed BLDC Motor Drive," IEEE Trans. Power Electron., vol.30, no.2, pp.871-887, Feb. 2015.

[8] L. Schrittwieser, J. W. Kolar, T. B. Soeiro, "99% Efficient Three-Phase Buck-Type SiC MOSFET PFC Rectifier Minimizing Life Cycle Cost in DC Data Centers," IEEE INTELEC International Telecommunications Energy Conference, pp.1-8, Oct. 2016.

[9] Jorge Garcia, Marco Antonio Dalla-Costa, André Luis Kirsten, David Gacio, Antonio J. Calleja, "A Novel Flyback-Based Input PFC Stage for Electronic Ballasts in Lighting Applications," IEEE Trans. Ind. Appl., vol.49, no.2, pp.769-777, Mar. 2013.

[10] Oscar García, José A. Cobos, Roberto Prieto, Pedro Alou, Javier Uceda, "Single Phase Power Factor Correction: A Survey," IEEE Trans. Power Electron., vol.18, no.3, pp.749-755, May 2003.

[11] Fernando Beltrame, Leandro Roggia, Luciano Schuch, José Renes Pinheiro, "A Comparison of High Power Single-Phase Power Factor Correction Pre-Regulators," IEEE ICIT Industrial Technology, pp.625-630, Mar. 2010.

[12] João Paulo M. Figueiredo, Fernando L. Tofoli, Bruno Leonardo A. Silva, "A Review of Single-Phase PFC Topologies Based on The Boost Converter," IEEE INDUSCON International Conference on Industry Applications, pp.1-6, Nov. 2010.

[13] Chan-Song Lee, Jin-Beom Jeong, Baek-Haeng Lee, Jin Hur, "Study on 1.5 kW Battery Chargers for Neighborhood Electric Vehicles," IEEE VPPC Vehicle Power and Propulsion Conference, pp.1-4, Sept. 2011.

[14] Hao Ma, Yue Ji, Ye Xu, "Design and Analysis of Single-Stage Power Factor Correction Converter With a Feedback Winding," IEEE Trans. Power Electron., vol.25, no.6, pp.1460-1470, June 2010.

[15] Gerry Moschopoulos, "A Simple AC–DC PWM Full-Bridge ConverterWith Integrated Power-Factor Correction," IEEE Trans. Ind. Electron., vol.50, no.6, pp.1290-1297, Dec. 2003.

[16] Mehdi Narimani, Gerry Moschopoulos, "A Three-Level Integrated AC–DC Converter," IEEE Trans. Power Electron., vol.29, no.4, pp.1813-1820, Apr. 2014.

[17] Bo-Tao, Yim-Shu Lee, "Power-Factor Correction Using Cuk Converters in Discontinuous-Capacitor-Voltage Mode Operation," IEEE Trans. Ind. Electron., vol.44, no.5, pp648-653, Oct. 1997.

[18] Grover Victor Torrico-Bascopé, Ivo Barbi, "A Single Phase PFC 3 kW Converter Using a Three-State Switching Cell," IEEE Power Electronics Specialists Conference, vol.5, pp.4037–4042, June 2004.

[19] Huai Wei, Issa Batarseh, "Comparison of Basic Converter Topologies for Power Factor Correction," IEEE Proceedings of Southeastcon, pp.348-353, Apr. 1998.

[20] Jinhua Liu, Xuejun Ma, "A Novel Topology Family of Single stage ACDC Converter with PFC," IEEE PEDG Power Electronics of Distributed Generation, pp.162-166, June 2010.

[21] André De Bastiani Lange, Thiago Batista Soeiro, Márcio Silveira Ortmann, Marcelo Lobo Heldwein, "Three-Level Single-Phase Bridgeless PFC Rectifiers," IEEE Trans. Power Electron., vol.30, no.6, pp.2935-2949, June 2015.

[22] Yungtaek Jang, Milan M. Jovanovic, "Bridgeless Buck PFC Rectifier," IEEE APEC Applied Power Electronics Conference, pp.23-29, Feb. 2010.

[23] Wang Wei, Liu Hongpeng, Jiang Shigong, Xu Dianguo, "A Novel Bridgeless Buck-Boost PFC Converter," IEEE PESC Power Electronics Specialists Conference, pp.1304-1308, June 2008.

[24] Krishna Kumar Gupta, Alekh Ranjan, Pallavee Bhatnagar, Lalit Kumar Sahu, Shailendra Jain, "Multilevel Inverter Topologies With Reduced Device Count: A Review," IEEE Trans. Power Electron., vol.31, no.1, pp.135-151, Jan. 2016.

[25] A. Pandey, B. Singh, B. N. Singh, A. Chandra, K. Al-Haddad, D. P. Kothari, "A Review of Multilevel Power Converters," Journal of the Institution of Engineers, vol.8, pp.220-231, Mar.2006.

[26] Suman Debnath, Jiangchao Qin, Behrooz Bahrani, Maryam Saeedifard, Peter Barbosa, "Operation, Control, and Applications of theModular Multilevel Converter: A Review," IEEE Trans. Power Electron., vol.30, no.1, pp.37-53, Jan. 2015.

[27] Alireza Nami, Jiaqi Liang, Frans Dijkhuizen, Georgios D. Demetriades, "Modular Multilevel Converters for HVDC Applications: Review on Converter Cells and Functionalities," IEEE Trans. Power Electron., vol.30, no.1, pp.18-36, Jan. 2015.

[28] Hani Vahedi, Philippe-Alexandre Labbé, Hadi Y. Kanaan, Handy Fortin Blanchette, Kamal Al-Haddad, "A New Five-Level Buck-Boost Active Rectifier," IEEE ICIT International Conference on Industrial Technology, pp.2559-2564, Mar. 2015.

[29] Vítor Monteiro, Andrés A. Nogueiras Meléndez, João C. Ferreira, Carlos Couto, João L. Afonso, "Experimental Validation of a Proposed Single-Phase Five-Level Active Rectifier Operating with Model Predictive Current Control," IEEE IECON Industrial Electronics Conference, pp.3939-3944, Nov. 2015.

[30] P. Roshankumar, P. P. Rajeevan, K. Mathew, K. Gopakumar, Jose I. Leon, Leopoldo G. Franquelo, "A Five-Level Inverter Topology with Single-DC Supply by Cascading a Flying Capacitor Inverter and an H-Bridge," IEEE Trans. Power Electron., vol.27, no.8, pp.3505-3512, Aug. 2012.

[31] Liangzong He, Chen Cheng, "A Flying-Capacitor-Clamped Five-Level Inverter Based on Bridge Modular Switched-Capacitor Topology," IEEE Trans. Ind. Electron., vol.63, no.2, pp.7814-7822, Dec. 2016.

[32] Vítor Monteiro, João C. Ferreira, Andrés A. Nogueiras Meléndez, João L. Afonso, "Model Predictive Control Applied to an Improved Five-Level Bidirectional Converter," IEEE Trans. Ind. Electron., vol.63, no.9, pp.5879-5890, Sept. 2016.

[33] Masoud Karimi-Ghartemani, "Linear and Pseudolinear Enhanced Phased-Locked Loop (EPLL) Structures," IEEE Trans. Ind. Electron., vol.61, no.3, pp.1464-1474, Mar. 2014.